RE-PENETRATION OF A SPUDCAN ON SAND NEAR AN EXISTING FOOTPRINT

Yung-Show Fang [1*], Cheng Liu [2], and Ying-Chu Shih [3]

ABSTRACT

This paper presents analytical and experimental data associated with the re-penetration of a spudcan on sand near an existing footprint. The instrumented 1-g physical model spudcan testing facility was used to investigate the variation of vertical reaction force, horizontal reaction force, and reaction moment on the spudcan with increasing penetration depth. The diameter D of the conical spudcan was 200 mm, and saturated loose Ottawa sand was used as the seabed material. Based on the experimental data, the following conclusions were drawn. For the first penetration of the spudcan, the measured vertical reaction force on the spudcan was in fairly good agreement with the theoretical solution calculated with the design guideline by the Society of Naval Architects and Marine Engineers (SNAME 2008). For the re-penetration with an offset distance equal to zero at the penetration depth from 0 to $0.1D$, due to the existence of the footprint depression, the spudcan was in a "stamp-on-void" condition, and all measured reactions on the spudcan were zero. However, after the bearing spudcan surface was embedded in soil at the penetration depth of $0.15D$, since the footprint soil had been heavily compressed and sheared during the first penetration, the measured vertical reaction increased rapidly with increasing depth of penetration. For the re-penetration with an offset distance of $0.5D$ at the penetration depth of zero, the spudcan-footprint interaction was similar to the loading of a footing on or near a slope. However, with the same offset distance at the penetration depth of $0.2D$, the induced soil behavior was similar to the general shear failure below a shallow foundation. The unusual reversal of horizontal reaction and reaction moment measured with increasing depth was induced by different failure mechanisms in foundation soil at different penetration stages. When the offset distance was greater than twice the spudcan diameter, the effects of the existing footprint disappeared. For the re-penetration of spudcan on sand, the critical offset distance varied between $0.25D$ and $0.5D$. The critical offset distance was influenced by both the penetration depth and the type of seabed soil.

Key words: Failure mechanism, footprint, model test, re-penetration, sand, spudcan.

1. INTRODUCTION

A turbine installation vessel (TIV) is a self-elevating platform specially designed for the installation of offshore wind turbines. To enable quick relocation in the wind farm, it is self-propelled. It has a slender ship shaped hull to achieve a quick turnaround time with the vessel carrying several foundations or wind turbines each time. A typical TIV consists of a floatable hull and four or six independent retractable legs that can be in excess of 90 m in length. The legs rest on spudcan footings that are usually circular or rectangular in plan. For TIV, the diameter of spudcan range from 5 to 20 m (Yi *et al.* 2012).

Once a TIV reaches the site, its installation begins by lowering the legs to the seabed and pushing the spudcan into the soil, while elevating the hull above the water. The spudcan footings are then pre-loaded by the two-point penetration method, which will be introduced in section 2.2 of this article. After the work of the TIV has finished, it is removed from the site after retracting

the legs from the seabed. This leaves a permanent seabed depression at each footing site, which is referred to as a "footprint". The installation, operation, and removal of the spudcan can remold the surrounding soil, resulting in highly variable shear strength profiles in the vicinity of the footprints (Gan *et al.* 2012).

With the installation of the foundation and wind turbine, the TIV might have to return to the same site for additional work. Therefore, they need to be reinstalled close to footprints previously left on the seabed. During this reinstallation, the spudcan are subjected to large eccentric and inclined loading conditions, resulting from the uneven seabed and the strength heterogeneity within the footprint. The jack-up installation is subjected to hazards including forces exceeding the structural capacity of the leg, excessive leg tilt, and potentially leads to structural failure (Kong *et al.* 2013).

Dier *et al.* (2004) reported incidents involving jack-up footing issued from 1957 to 2002. In these cases, about one third of jack-up accidents were associated foundation problems. These foundation problem histories were classified to categories such as: punch-through (53%), uneven seabed/scour/footprint (15%), seafloor instability/mudslide/seabed slide/volcanic activity (15%), sliding of mat foundation (10%), unexpected penetration (8%), and others (8%). Punch-through has the highest occurrence rate 53% in all 56 incidents. The second highest incident rate 15% was due to the combination of uneven seabed, scour, and footprint.

Based on the work of Osborne (2005), Hortono *et al.* (2014)

reported a survey on incidents related to geotechnical aspects of jack-up units. There was an increasing trend of incidents related to spudcan-footprint interaction from 3% in the period 1979 ~ 1988 to 9% in the period 1996 ~ 2005. Interestingly, there was a declining trend of incidents related to spudcan punch-through, from 42% in the period of 1979 ~ 1988 to 16% in the period of 1996 ~ 2005. It is clear that, except punch-through, uneven seabed/scour/footprint is the most important reason to cause an incident for jack-up foundation.

This paper presents experimental data associated with the footprints and reactions induced by the re-penetration of a spudcan near an existing footprint. Based on the test data, the footprint-spudcan interaction and failure mechanism of surrounding seabed soil were carefully investigated. All experiments mentioned in this paper were conducted in the National Chiao Tung University (NCTU) 1-g model spudcan testing facility, which was briefly described in the following sections. Saturated loose Ottawa sand was used as the seabed material. In Fig. 1, the diameter D of the model spudcan was 200 mm. Penetration resistance on the spudcan was measured by a six-component force transducer. The offset distance from the center of footprint to the center of spudcan included 0, $0.125D$, $0.25D$, $0.5D$, $1.0D$, $1.5D$, and $2.0D$. It was hoped that these test results would enhance a better understanding regarding the spudcan-soil interaction during its re-penetration near an existing footprint.
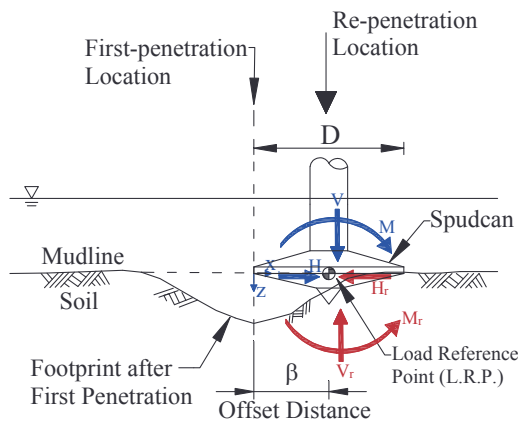

Fig. 1   Footprint after first penetration and definition of offset distance

2.   PENETRATION DEPTH OF SPUDCAN

Based on the design guideline proposed by the Society of Naval Architects and Marine Engineers (SNAME 2008), this section studied the factors affecting the penetration depth of a spudcan on sand. The analysis was based on the general bearing capacity equation of a footing originally developed by Meyerhof (1963), and later adopted by the SNAME (2008).

2.1   Penetration Resistance Estimation by SNAME

In 2008, the Technical and Research Bulletin 5-5A relating to the site-specific assessment of mobile jack-up unit was published by SNAME. In Section C6.2.3 of the Bulletin, it was described that the ultimate vertical bearing capacity F_v of a circular footing resting in silica sand or other granular materials could be computed by the following equation:

$$F_v = A\,(0.5\gamma' B\,N_\gamma\,s_\gamma\,d_\gamma + p_o'N_q\,s_q\,d_q) \tag{1}$$

In Eq. (1), A = spudcan effective bearing area, p_o' = effective overburden pressure at the depth of bearing area, s_γ, s_q = shape factors, d_γ, d_q = depth factors. At the end of Section C6 of SNAME (2008), the factors in Eq. (1) were defined as follows:

$$N_\gamma = 2(N_q + 1)\tan\phi \tag{2}$$

$$s_\gamma = 1-0.4\left(\frac{B}{L}\right) \quad (=0.6 \text{ for circular footing}) \tag{3}$$

$$d_\gamma = 1 \tag{4}$$

$$N_q = e^{\pi\tan\phi}\tan^2(45+\phi/2) \tag{5}$$

$$s_q = 1+\left(\frac{B}{L}\right)\tan\phi \tag{6}$$

$$d_q = 1 + 2\tan\phi\,(1-\sin\phi)^2\,(D/B) \qquad \text{(for } D/B \leq 1)$$
$$= 1 + 2\tan\phi\,(1-\sin\phi)^2\arctan(D/B) \qquad \text{(for } D/B >1) \tag{7}$$

In these equations, ϕ = angle of internal friction for sand (degrees), B = effective spudcan diameter, L = foundation length (for circular foundation $L = B$), D = distance from mudline to spudcan maximum bearing area. In this study, the theoretical penetration resistance of the spudcan was calculated with Eq. (1). It should be mentioned that, in this investigation, the diameter of spudcan was defined as D instead of B as indicated in Fig. 1, and the depth of spudcan penetration was defined as z instead of D. The vertical force acting on the circular spudcan was defined as V instead of F_v. Based on their experimental study for a model spudcan penetrating loose and dense sand, Fang *et al.* (2019) reported that the measured penetration resistance was in fairly good agreement with the theoretical prediction estimated with SNAME (2008).

The vertical force V, horizontal force H, and bending moment M acting on the spudcan re-penetrating the seabed near an existing footprint are shown in Fig. 1. The vertical reaction force V_r, horizontal reaction force H_r, and reaction moment M_r acting on the spudcan are also illustrated in Fig. 1. Since the granular soil cannot resist tension, the sign convention for vertical force is positive for compression. In this study, the horizontal force is defined as positive if it acts in the x-axis direction. In Fig. 1, the bending moment is defined as positive if it trends to rotate the spudcan about its load reference point (L.R.P.) in the counterclockwise direction.

2.2   Theoretical Estimate of Penetration Depth

Assuming the theoretical Eq. (1) proposed by SNAME (2008) was correct, this section investigated the factors affecting the penetration depth z of spudcan due to the load application of a turbine installation vessel. The estimated penetration depth range would be adopted for the model experiments in this article.

In 2017, two demonstration offshore wind turbines were installed at the Formosa I wind farm, off the west coast of Miaoli County in Taiwan. The wind turbines with the capacity of 4.0 MW each were delivered by Siemens Gamesa and installed by Swancor. Figure 2 showed the construction of the transition piece between the foundation and tower with the TIV. Marine Traffic (2017) indicated, the weight of the TIV named Torben used for

construction was about 116 MN. The TIV was capable of carry eight offshore wind turbines. Each turbine, mainly included the blade, nacelle, and tower, weighted about 4.0 MN. The total weight of the TIV and eight turbines would be about 148 MN.

Figure 2 showed the jack-up platform had four legs. To apply the preloading factor of 2.0 during initial TIV setting, two spudcan would penetrate into the seabed soil (two-point penetration method), while the other spudcan remained barely touching the soil surface. Then the loading on the first two legs were gradually released, and the other two legs were pressed progressively into the seabed soil. Under the preloading factor of 2.0, the total weight of the TIV and the payload was shared by only two spudcan. For this case, each spudcan carried an ultimate vertical force of 74 MN during penetration.

The subsurface investigation report by the Taiwan Power Company (2009) indicated that, the seabed soils on the west coast of Taiwan at Changhua wind farm were interlayers of silty sand and silty clay. For the sandy soils in bore holes BH-04 and BH-09, the measured blow counts from standard penetration tests varied from 7 to 21. The corresponding relative density ranged from 15 to 46%. Based on Das and Sobhan (2018), the sedimentary cohesionless soil at Changhua wind farm was very loose to loose. For the silty sand samples obtained from the site, direct shear test results indicated its internal friction angle varied from 27.0° to 32.6°, and the average value was 28.9°.
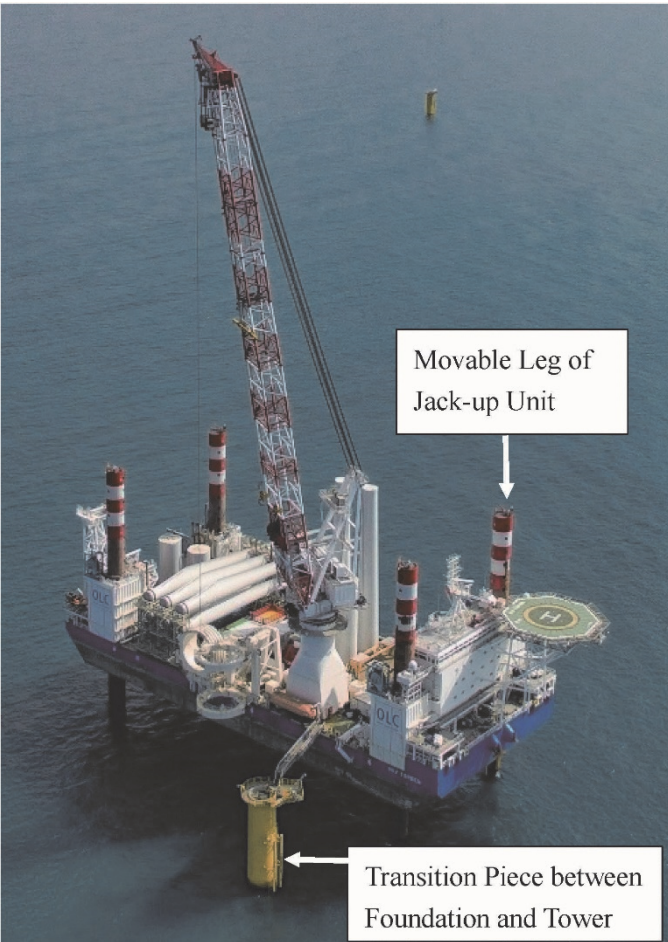
2.2.1 Effects of Spudcan Diameter

Assuming that Eq. (1) suggested by SNAME (2008) was correct, this study investigated effects of spudcan diameter and shear strength of soil on induced penetration depth. The penetration depth z was defined as the distance from the mudline to the maximum bearing area of the spudcan. Figure 3(a) showed the change of calculated vertical force V with normalized penetration depth z/D, for the spudcan with diameters 9.0, 10.0, 10.7, and 11.0 m. For the cohesionless soils at Changhua wind farm, the average internal friction angle was 28.9°, and the average saturated unit weight was 19.27 kN/m³. In Fig. 3(a), if the spudcan diameter was 10.0 m, under the vertical load of 74 MN, the induced penetration depth would be $0.161D$. Construction data at
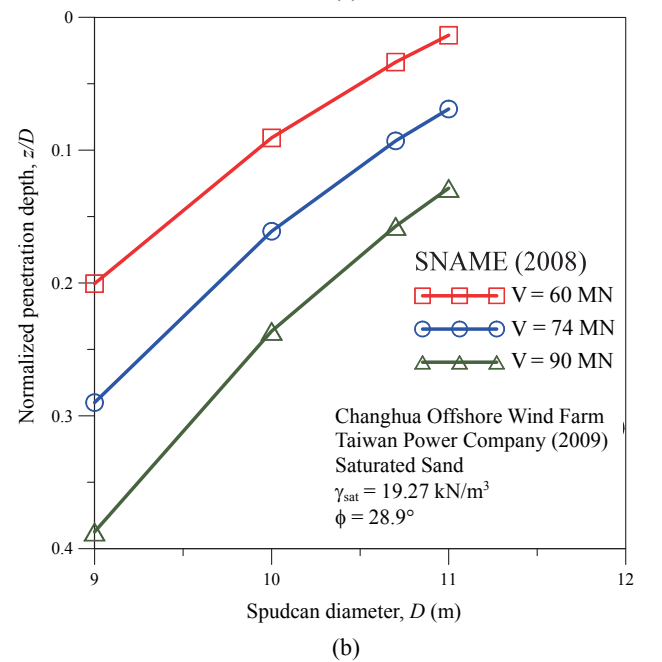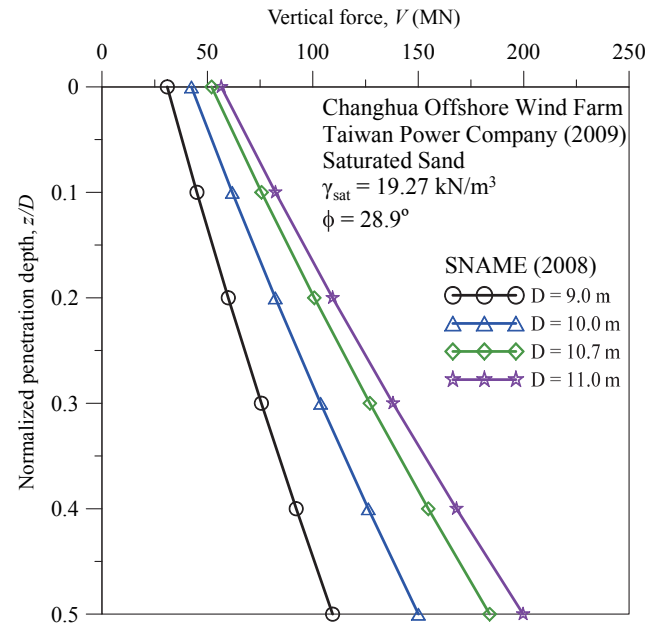

Fig. 2   Wind turbine installation vessel with jack-up unit (after Swancor 2017)

Fig. 3   Effects of spudcan diameter on penetration resistance V_z and penetration depth z

the Formosa I wind farm indicated that the area of the spudcan used was 90 m². If the spudcan was conical, the corresponding diameter should be $D = 10.7$ m. Under the application of $V = 74$ MN, the induced penetration depth should be $z = 0.093D = 1.00$ m. However, if a spudcan with the diameter $D = 11.0$ m was used, the estimated penetration depth would be $z = 0.069D = 0.76$ m. Figure 3(b) showed the decrease of penetration depth of the spudcan with increasing spudcan diameter, under the vertical forces $V = 60$, 74, and 90 MN.

2.2.2   Effects of Soil Strength

For the spudcan with a diameter 10.7 m, Fig. 4(a) illustrated the distribution of vertical force V with penetration depth for seabed soils with internal friction angles ranging from 26º to 34º.
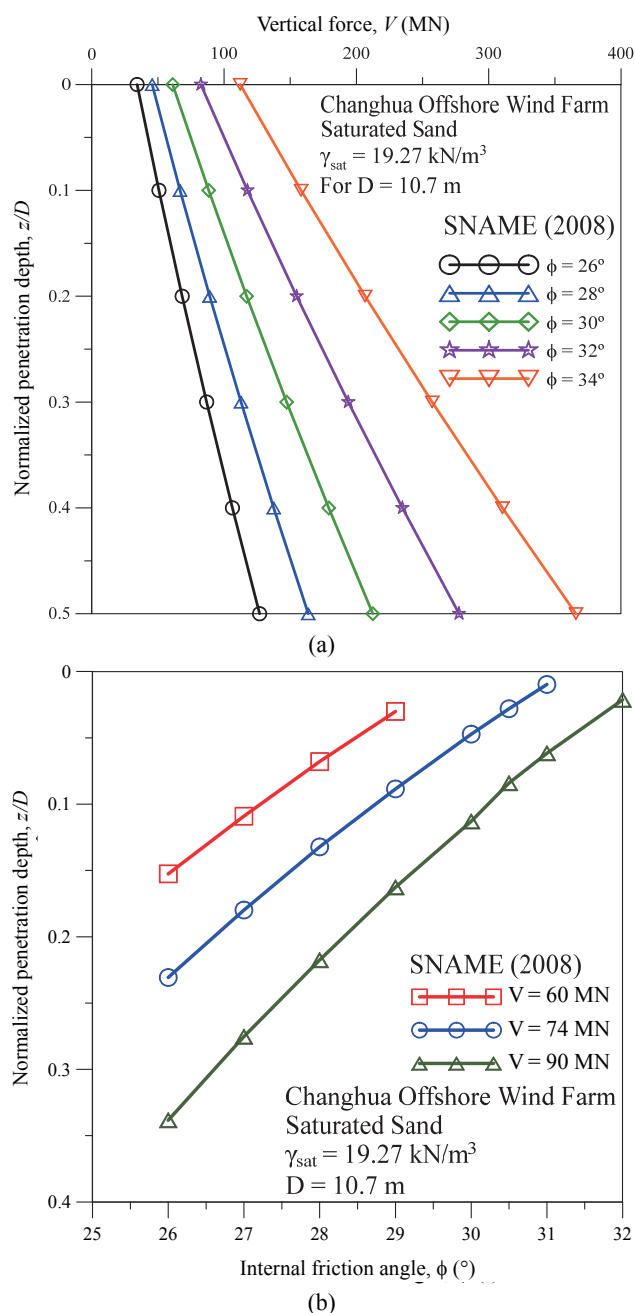

Fig. 4   Effects of internal friction of sand on penetration resistance V_z and penetration depth z

For the silty sand at the Changhua wind farm, the internal friction angle varied from 27.0º to 32.6º. In Fig. 4(b), under the vertical loading $V = 74$ MN, for $\phi = 27º$, 28º, 29º, 30º and 31º, the corresponding penetration depth z/D would be 0.180, 0.132, 0.088, 0.047, and 0.010, respectively. This was how the maximum penetration depth $z_{max} = 0.2D$ for all model experiments in this study was selected. Assuming the bearing capacity equation developed by Meyerhof (1963) and the design formula by SNAME (2008) was correct, the actual penetration of spudcan in sand should be less than 0.2D.

It was found from Figs. 3(b) and 4(b) that the induced penetration depth of spudcan in sand was significantly influenced by the spudcan diameter, the vertical force applied, and the shear strength of soil. It could also be observed from these data that, since the granular soil was relative stiff when compared with soft clay, therefore the induced penetration depth of the spudcan was constrained to a limited extent (for $V = 74$ MN and $D = 10.7$ m, $z = 0.093D$ in Fig. 3(b)). Based on his centrifuge experimental results, a similar observation was also reported by Hartono (2014). Osborne *et al.* (2011) reported, for a spudcan penetrating soft to firm clay or loose silt seabed, the amount of penetration could reach 0.5D to 2.0D, for a spudcan penetrating seabed with uniform sand, the amount of penetration would be minimal. It could be summarized that, the most important factor affecting the penetration depth of spudcan was the type of seabed soil. From a practical point of view, for the model experiments in the fifth part of this paper, it was focused on the spudcan penetration depth of $z = 0.10D$, 0.15D, and 0.20D.

3.   NCTU MODEL SPUDCAN TESTING FACILITY

To investigate the spudcan-seabed interaction, a 1-g physical model facility was designed and constructed at the National Chiao Tung University. The entire facility consisted of four components, namely, vertical force loading system, soil bin, model spudcan, and data acquisition system, which was briefly introduced as follows.

3.1   Vertical Force Loading System

Figure 5 showed, above the soil bin, a steel reaction frame was constructed to resist the reaction forces and bending moments induced during the penetration of spudcan. The reaction frame was made of four steel columns, two horizontal steel H-beams, and two movable horizontal steel beams.

The vertical force loading device indicated in Fig. 5 was used to push down and lift up the model spudcan during testing. The capacity of the loading machine was 100 kN, and its maximum stroke was ±450 mm. A speed control panel was used to control the descending and ascending speed of the model spudcan. Following the laboratory studies by Martin and Houlsby (2000), and Hossain *et al.* (2006), both upward and downward speeds of the model spudcan were controlled to 0.34 mm/s in this study.

A 6-component force transducer (Kyowa, LFX-A-3kN) was used to measure the application of forces and moments on the spudcan during its penetrating and uplifting. The transducer was capable of simultaneous measurement of three components of forces (H_x, H_y, V_z) and 3 moments (M_x, M_y, M_z). However, for this
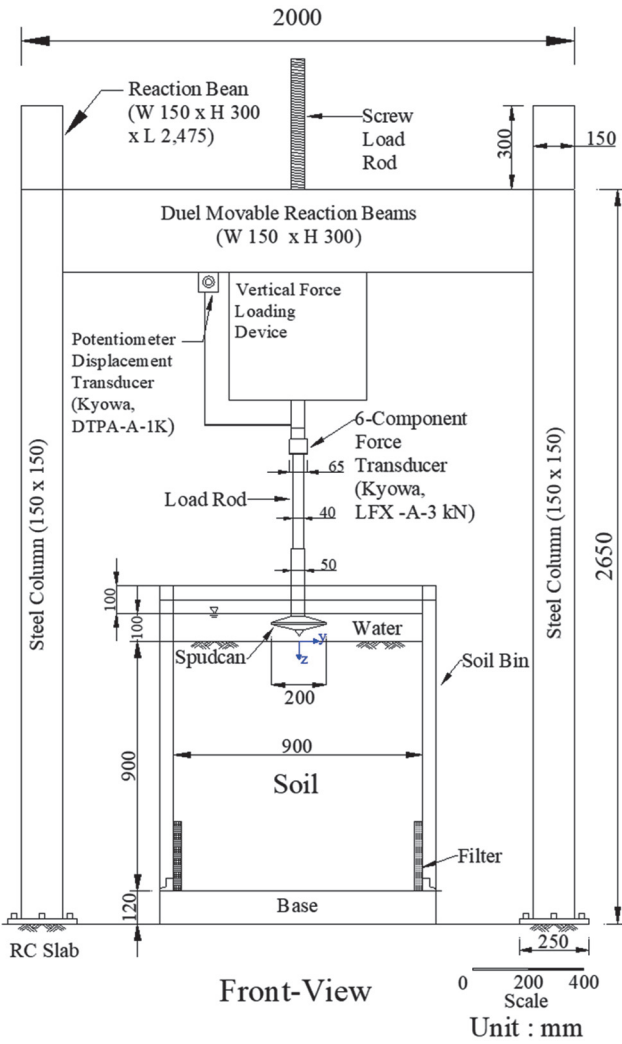
Fig. 5   Loading system with reaction frame

study only the vertical force *V*, horizontal force *H*, and bending moment *M* illustrated in Fig. 1 were measured. The capacity of vertical force, horizontal force, and bending moment for this load cell was 3 kN, 3 kN, and 100 N-m, respectively.

A potentiometer-type displacement transducer (Kyowa, DTPA-A-1K) was used to measure the downward and upward displacement of the model spudcan. The rated capacity of this transducer was 1,000 mm. In Fig. 5, the displacement transducer was mounted on the movable reaction beam. Before testing, a stainless steel wire was pulled out from the transducer to an extension rod connected to the load rod. With the penetration of spudcan into soil, the load rod moved down, and the wire was pulled out accordingly.

3.2   Soil Bin

In this study, the diameter of the conical model spudcan was 200 mm. Figure 5 showed, below the model spudcan, there was a steel soil bin to contain the soil specimen. The inside dimensions of the rectangular bin were 900 mm-wide, 1,200 mm-long, and 1,100 mm-high. In Fig. 5, the height of soil specimen and water was 900 mm and 1,000 mm, respectively. The steel sidewalls, steel base plate, 18 box-type steel columns, and 20 steel beams were carefully welded together to ensure the stiffness of the bin.

Since the soil specimen was fully submerged during testing, the 5 mm-thick inner wall of the bin was made of stainless steel to prevent rusting.

To achieve a saturated condition for seabed soils, after the laboratory specimen was submerged, the air remained in the soil sample was removed by suction. To achieve an air-tight chamber, a 1,320 mm-long, 1,010 mm-wide, and 25 mm-thick steel cover-plate was made. After the soil specimen was pluviated, and inundated in the bin, the cover plate was placed on top of the soil bin. Then air trapped in the submerged soil was sucked out by a vacuum pump.

3.3   Model Spudcan

The shape and dimensions of the conical model spudcan used for all experiments in this investigation was illustrated in Fig. 6(a) and 6(b). The spudcan was made of steel and had a diameter of 200 mm. In this study, the depth of penetration of the spudcan was defined for the amount of penetration of the load reference point shown in Fig. 6(a). Figure 7 showed the movable reaction beam, loading device, force transducer, model spudcan, and soil bin of the NCTU model spudcan testing facility.
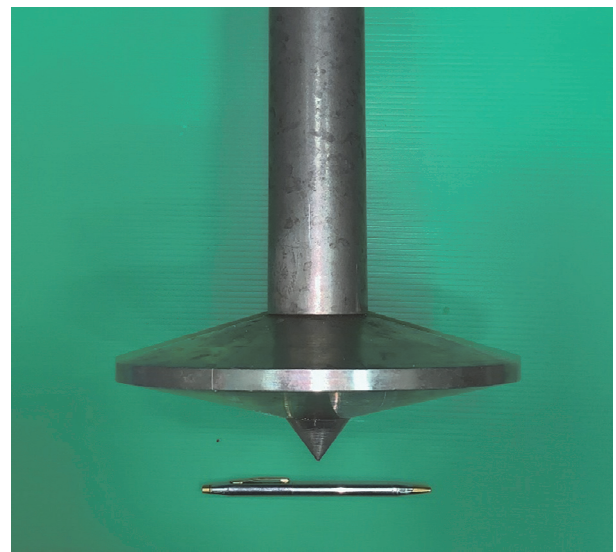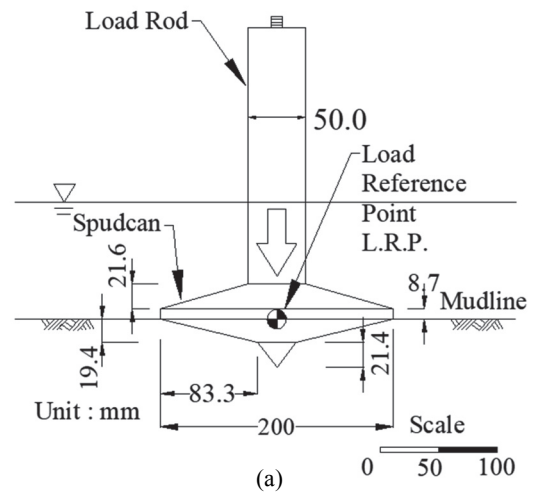

(a)

(b)

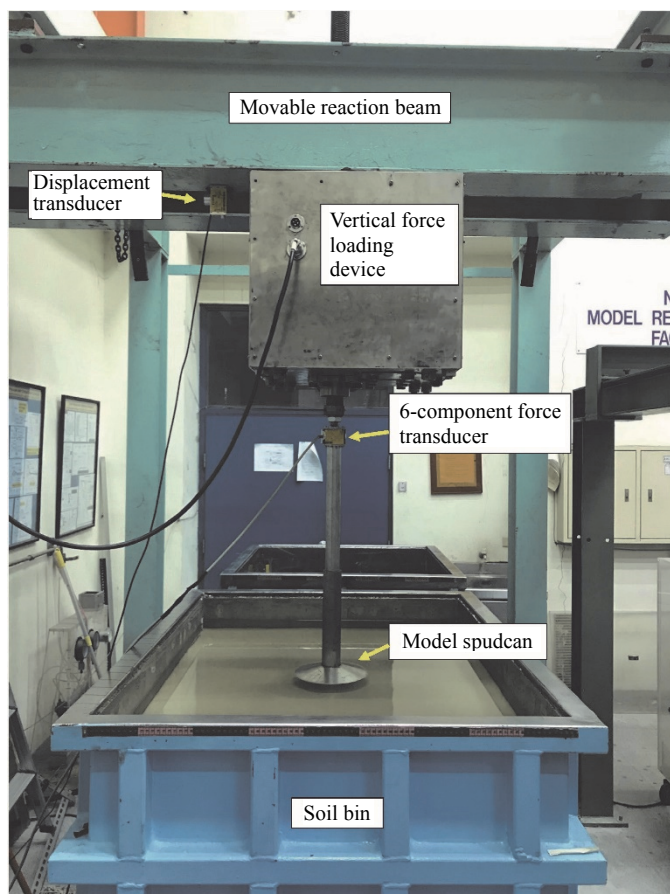**Fig. 6   Shape and dimensions of model spudcan**

Fig. 7   Model spudcan with force transducer and vertical force loading device

3.4   Data Acquisition System

Due to the considerable amount of data collected during the test, a data acquisition system was used. For the 6-componant force transducer, a dynamic strain amplifier was built in the load cell. The output analog signal was collected and digitized by the data logger (GRAPHTEC, GL240). The digitized data was then transmitted to the computer to obtain the vertical force V, horizontal force H, and bending moment M acting on the spudcan. For the potentiometer-type displacement transducer, the analog signal from the sensor was filtered and amplified by the dynamic strain amplifier (Kyowa, DPM-711B), then digitized by an analog-to-digital converter. The digitized signal was then transmitted to the computer for storage and analysis. For more information regarding the NCTU model spudcan testing facility, the reader is referred to Fang *et al.* (2019).

4.   SPECIMEN PREPARATION AND TEST PROCEDURE

Ottawa sand was used for all model experiments in this study. Physical properties of the soil included $G_s = 2.65$; $e_{max} = 0.76$; $e_{min} = 0.50$; $D_{60} = 0.39$ mm; and $D_{10} = 0.26$ mm. The Ottawa sand was classified as SP by the Unified Soil Classification System.

4.1   Specimen Preparation

The purpose of this investigation was to investigate the re-

sistance on a spudcan penetrating the seabed near an existing footprint. To achieve a loose seabed, air-dry Ottawa sand was deposited by air-pluviation from the slit of a hopper into the soil bin. The slot opening of the hopper was 10 mm, and the drop distance was approximately 0.2 m from the soil surface throughout the placement process. The air-pluviation method had been widely used to reconstitute sand samples in the laboratory. Rad and Tumay (1987) reported that pluviation method provides reasonably homogeneous specimens with desired relative density. Lo Presti *et al.* (1992) concluded that the pluviation method is an efficient way of preparing large soil sample.

Density control molds were used to evaluate the variation of soil density in the soil specimen. The cylindrical mold had an inner diameter of 152.4 mm and a height of 155.2 mm (ASTM D4254, 2014). It was found that the air-dry soil density was quite uniform in the soil mass. The mean relative density with one standard deviation was $D_r = 15.1 \pm 1.1\%$.

To simulate the behavior of seabed soils, the soil specimen should be saturated. After soil placement, water flowed into the soil bin, until the water surface rose to 100 mm above soil surface as illustrated in Fig. 5. After inundation, the relative density of soil increased significantly to about 25%. To remove the air trapped among soil particles, an air-tight cover plate was clamped to the top of the soil bin, then a suction of -50 kPa was applied by a vacuum pump for 8 hours. After suction, the relative density of soil rose slightly to $25.5 \sim 26.5\%$. Das and Sobhan (2018) stated, for granular soil deposits, the relative density between 15 and 50% was described as loose. The subsurface investigation report of Taiwan Power Company (2009) indicated, the relative density of the cohesionless seabed soils at the Changhua wind farm varied from 15 to 46%. It was obvious that the relative density $25.5 \sim 26.5\%$ of the prepared soil specimen was within the range of relative density in the field.

4.2   Test Procedure

4.2.1   First Penetration

After the soil specimen was properly prepared, the vertical force loading device and the movable reaction beam was moved to the location of first penetration as indicated in Fig. 8. Then the vertical loading device pushed the spudcan downward at the
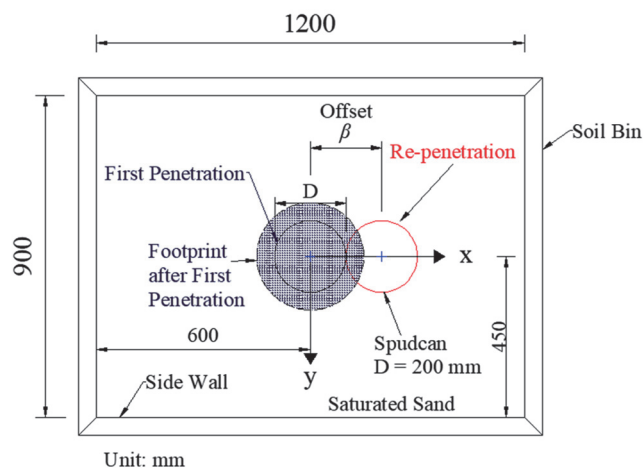

Fig. 8   Footprint after first spudcan penetration and location of re-penetration

speed of 0.34 mm/s. Figure 6 showed, as the L.R.P. reached the mudline, the penetration depth was equal to zero. When the desired penetration depth $z = 0.2D = 40$ mm was reached, the spudcan was retracted at the speed of 0.34 mm/s. After the spudcan was totally pulled out, the footprint profile was measured.

4.2.2 Re-Penetration

The movable reaction beam and the vertical loading device were moved to the location of re-penetration as illustrated Fig. 8. The horizontal offset distance adopted for his study included $\beta = 0$, $0.125D$, $0.25D$, $0.5D$, $1.0D$, $1.5D$, and $2.0D$. The vertical loading device once again pushed the spudcan downward at the speed of 0.34 mm/s. When the desired penetration depth $z = 0.2D$ was reached, the penetration stopped. Then the spudcan was retracted from soils, and the footprint profile on the seabed was measured. During the entire penetration, re-penetration, and retraction process, the reactions on the spudcan were measured by the six-component force transducer.

5. TEST RESULTS

This section reported the experimental results regarding the first penetration of a spudcan into level seabed, and the re-penetration of the spudcan near an existing footprint. The reactions acting on the spudcan during its penetration were carefully investigated. For all experiments in this study, the diameter D of the spudcan was 200 mm. The relative density of the sandy specimen varied from 25.5 to 26.5%. The average relative density was 26.0%, and the average unit weight was 19.37 kN/m³. Based on direct shear test results, the corresponding internal friction angle of the saturated loose sand was 31.7°.

5.1 First Penetration

Test results associated with the first penetration of the model spudcan on a level seabed were reported as follows.

5.1.1 Footprints

The footprint profiles measured after the first penetration of the spudcan were illustrated in Fig. 9. Before spudcan penetration, a horizontal L-shaped steel beam was placed on top frame of the soil bin, and a digital vernier caliper attached to the beam was used to measure the initial elevation profile of soil surface. After the spudcan was penetrated and pulled out, the elevation profile of soil surface was measured again by the same digital vernier caliper. The settlement or heaving of soil surface before and after spudcan penetration indicated the footprint profile. It was obvious that the settlement curves on the *xz* and *yz* sections were nearly identical. Since the model spudcan was conical, it was not surprising that the induced depression cone was axisymmetric. The maximum settlement in Fig. 9 was about 68 mm. The maximum settlement at the center of the footprint 68 mm included the combined contribution of the 40 mm spudcan penetration, lower cone height 19.4 mm, and the height of tip cone 21.4 mm. The diameter of the footprint in sand was about 300 mm. The volume change of the depression cone was induced by the compression of soils under the heavily loaded spudcan, and the volume contraction of the loose sand under shearing.
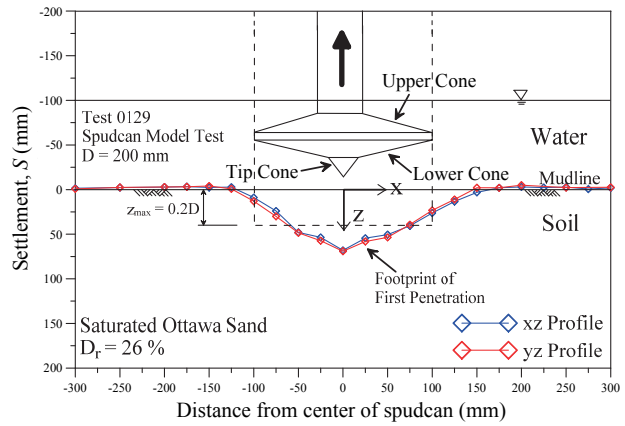

Fig. 9 Footprint after first penetration of spudcan

5.1.2 Reactions

In Fig. 10, the vertical reaction force V_r acting on the spudcan with increasing penetration depth z was represented by the black solid curve. When the 19.4 mm-thick (0.1D-thick) lower cone shown in Fig. 9 touched soil surface, the vertical reaction force V_r started to build up. At the penetration depth $z = 0$, the lower cone was buried in soil, and the vertical reaction measured was 0.26 kN. In Fig. 10, the vertical reaction increased with increasing penetration depth. At the end of penetration ($z = 0.2D$), the measured vertical reaction force was 1.08 kN. The ultimate bearing capacity of the spudcan with increasing depth estimated with SNAME (2008) was also plotted in Fig. 10. Considering all assumptions made by Meyerhof (1963), it was concluded that the measured vertical reaction was in fairly good agreement with the theoretical solution.

In Fig. 10, when the spudcan was extracted from the soils, the vertical reaction on the spudcan suddenly vanished. The upward moving spudcan was separated from discrete soil particles below. From a practical point of view, the vertical force on the spudcan throughout the extraction process could be considered as zero.
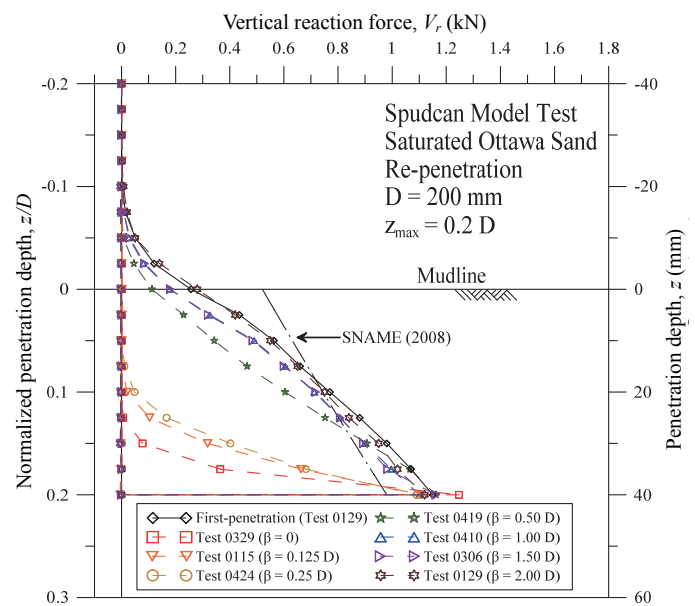

Fig. 10 Variation of vertical reaction with depth on spudcan due to re-penetration at different offsets

In Fig. 11, the black solid curve showed the variation of horizontal reaction force H_r on the spudcan with increasing penetration depth. Since the conical spudcan was axisymmetric, the measured horizontal forces during its first penetration were nearly zero. In Fig. 12, the solid black line showed the change of reaction moment M_r on the spudcan with increasing depth. The measured M_r values were nearly zero, because the first spudcan penetration was axisymmetric. If the prepared soil specimen was totally homogeneous, isotropic, and uniform, the H_r and M_r on the axisymmetric spudcan should equal to zero. It could be concluded that the measured horizontal reaction and reaction moment on the spudcan were negligible.
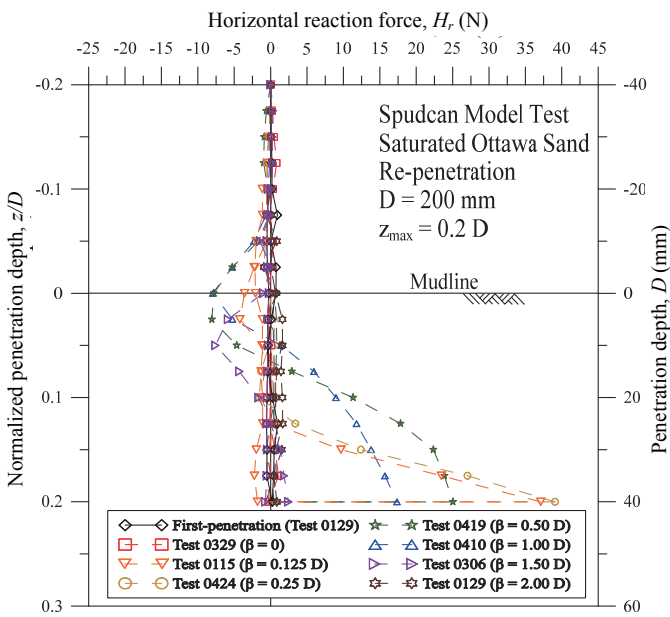

Fig. 11   Variation of horizontal reaction with depth on spudcan due to re-penetration at different offsets
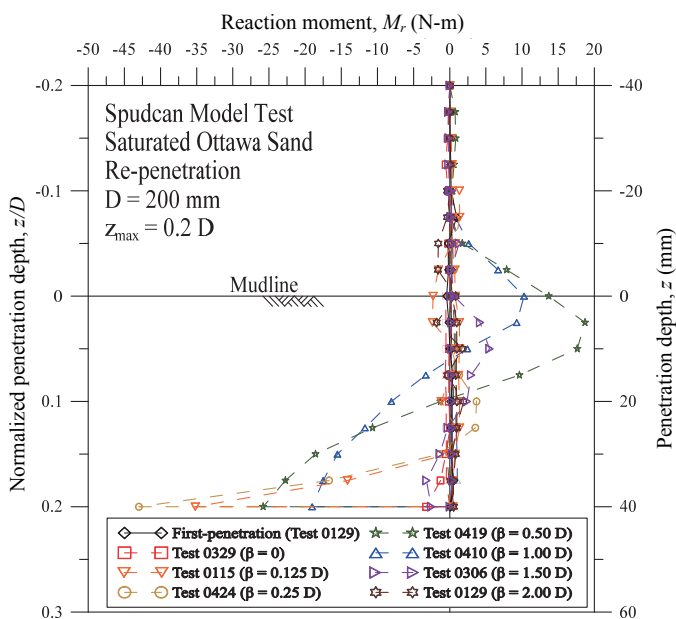

Fig. 12   Variation of reaction moment with depth on spudcan due to re-penetration at different offsets

5.2   Re-Penetration near an Existing Footprint

This section reported the vertical reaction force V_r, horizontal reaction force H_r, and reaction moment M_r on the spudcan penetrating the seabed near an existing footprint. The offset distance for model experiments included 0, 0.125D, 0.25D, 0.5D, 1.0D, 1.5D, and 2.0D.

5.2.1   Footprints

Figure 13 showed the footprints on the *xz*-section on the seabed after the first penetration and the re-penetration of the spudcan. In Fig. 13(a), the spudcan was first penetrated and re-penetrated at the same location. In the figure, the same cylindrical zone had been disturbed twice, and the final footprint was almost identical to that induced by the first penetration. In Fig. 13(b), the offset distance was 0.25D. During re-penetration, the loose sand below the footing on the right were compressed and sheared. Therefore, more surface settlements were induced on the offset-skirt of the existing footprint. In Fig. 13(c), the offset distance was 0.5D. When the spudcan was pushed down 0.2D during re-penetration, most probably a general shear failure developed toward the footprint, and soils moved along the failure
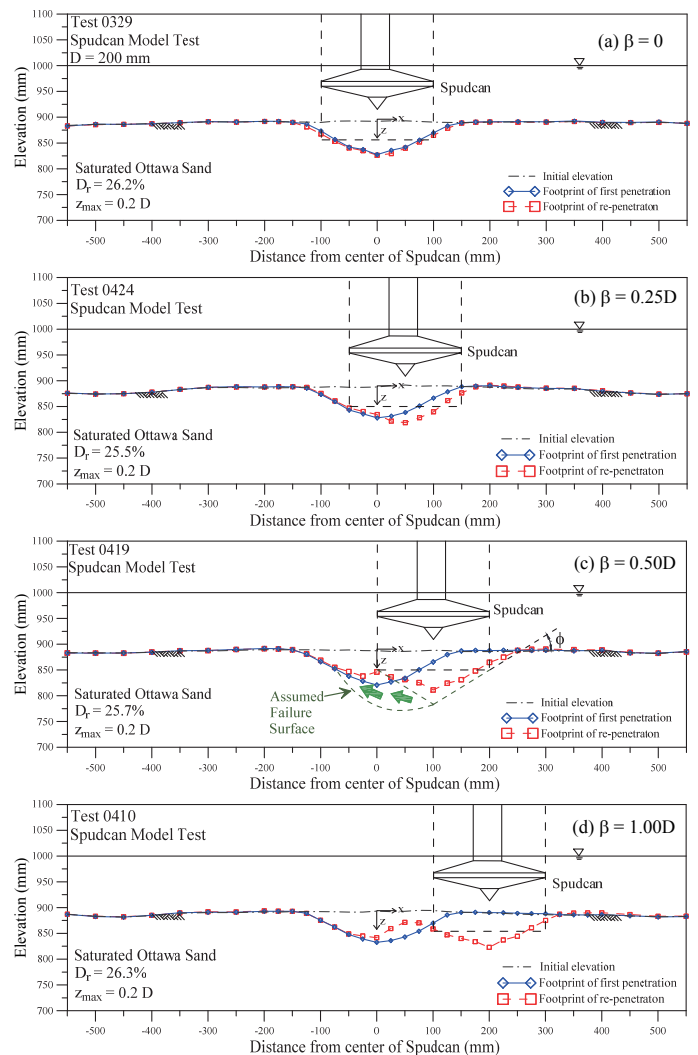

Fig. 13   Footprint on *xz* section after re-penetration of spudcan at different offset locations

surface. The passive Rankine wedge pushed the soil to fill the existing footprint. In Fig. 13(d) for β = 1.0*D*, the tendency for the passive soil wedge to the fill the footprint depression was still evident. However, an independent footprint induced by the re-penetration became more evident.

Figure 14 showed the footprints on the *yz*-section at *x* = β after re-penetration of the spudcan. Based on these test data, it could be concluded that, from β = 0 to 2.0*D*, all settlement profiles on the *yz*-section were nearly identical.

Figure 15(a) to 15(h) illustrated the interaction between the spudcan and the footprint soil. The footprint profiles in the figures were measured at the beginning and at the end of the re-penetration. These figures were used to interpret the measured reactions on the spudcan at the penetration depths of 0 and 0.2*D*.
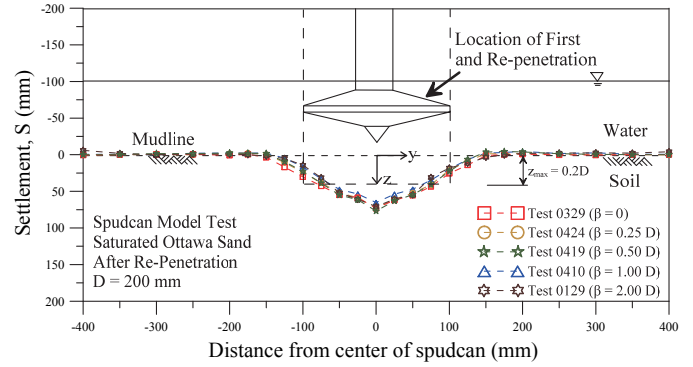

Fig. 14 Footprint on *yz* section at *x* = β after re-penetration of spudcan at different offset locations
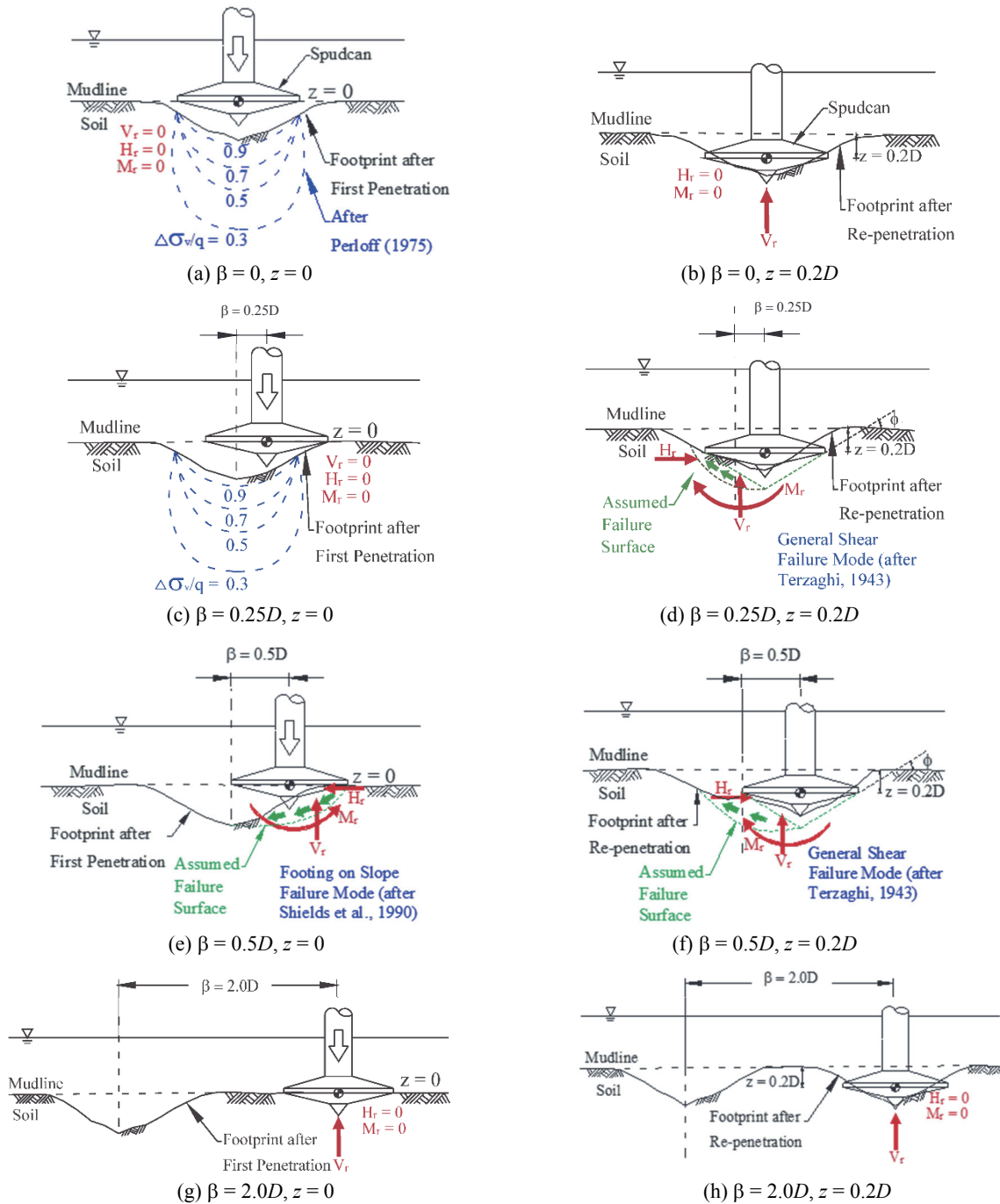

Fig. 15 Mechanism of a spudcan re-penetrating seabed near an existing footprint

5.2.2　Vertical Reaction

The variation of vertical reaction force V_r on the spudcan with penetration depth for $\beta = 0$ was indicated in Fig. 10 with the red dashed curve. In Fig. 15(a), for $\beta = 0$ and $z = 0$, the spudcan was actually hanging at the center of the footprint generated by the first penetration. In Fig. 10, for $\beta = 0$, due to the existence of the footprint depression, the spudcan was in a "stamp-on-void" condition, the measured vertical reaction was equal to zero from the depth $z = 0$ to $0.1D$. However, when the bearing surface of spudcan was embedded in soil at the penetration depth of $0.15D$, because the footprint soil had been heavily compressed and sheared during the first penetration, the measured vertical reaction force V_r increased rapidly with increasing depth of penetration. In Fig. 10, at the penetration depth of $0.2D$, the measured vertical force was nearly the same as that due to the first penetration.

This extraordinary phenomenon could be explained with Fig. 15(a) and 15(b). The contour of vertical normal stress increment $\Delta\sigma_v$ beneath a uniformly loaded circular area on a linearly elastic half-space introduced by Perloff (1975) was indicated in Fig. 15(a). During the re-penetration of the spudcan at $z = 0$, as indicated in Fig. 15(a), the spudcan was not touching the footprint surface. Therefore, no vertical reaction force was recorded. At the penetration depth $z = 0.20D$, as shown in Fig. 15(b), the maximum bearing area of the spudcan was in full contact with footprint soil, which had been heavily compressed and sheared during the first penetration. Due to the compression and shearing, the footprint soil contracted, and its stiffness and shear strength increased. This is the main reason why the measured V_r increased rapidly with increasing penetration depth. In Fig. 10, a similar vertical reaction behavior could be observed on the test results for $\beta = 0.125D$ and $\beta = 0.25D$.

The variation of the vertical reaction V_r on the spudcan with increasing penetration depth for $\beta = 1.0D$ was illustrated in Fig. 10 with the green dashed curve. Since the location of re-penetration was relatively far from the existing footprint, the effects of the existing footprint became less significant. As a result, the vertical reaction on the spudcan converged to that for the first penetration.

In Fig. 15(g) and 15(h), the re-penetration location was far away ($\beta = 2.0D$) from the existing footprint. Therefore, the V_r vs. z curve for re-penetration should be identical to that for the first penetration. In Fig. 10, for $\beta = 2.0D$, the measured V_r *vs.* z relationship (brown dashed curve) was nearly the same as that for the first penetration.

5.2.3　Horizontal Reaction and Reaction Moment

The horizontal reaction force H_r and reaction moment M_r on the spudcan were related, therefore H_r and M_r were discussed together in this section. The test results regarding the variation of H_r and M_r with penetration depth was a little confusion, therefore Fig. 15(a) to 15(h) were used to help to illustrate the spudcan-footprint interaction.

In Fig. 15(a), for the case with offset distance $\beta = 0$ and penetration depth $z = 0$, the spudcan was in a "stamp-on-void" condition. The spudcan did not touch the footprint surface, as a result the H_r and M_r on the spudcan should be zero. The variation of horizontal reaction H_r and reaction moment M_r with depth for

the $\beta = 0$ condition were indicated in Fig. 11 and 12 with red dashed curves. At the penetration depth $z = 0$, the measured H_r and M_r were zero.

In Fig. 15(b), for the case $\beta = 0$ and $z = 0.2D$, the re-penetration was conducted at the same location as the first penetration. Since both penetration were axisymmetric, the measured H_r and M_r should be zero. In Fig. 11 and 12, for $\beta = 0$ and $z = 0.2D$, the recorded H_r and M_r were negligible.

In Fig. 15(c), for the case $\beta = 0.25D$ and $z = 0$, the edge of the spudcan was barely touching the mudline. The "stamp-on-void" situation still existed, therefore all reactions on the spudcan should be zero. The variation of H_r and M_r with depth for the $\beta = 0.25D$ condition were displayed in Fig. 11 and 12 with yellow dashed curves. At the penetration depth $z = 0$, the measured H_r and M_r were zero.

In Fig. 15(d), for the case $\beta = 0.25D$ and $z = 0.2D$, the bearing surface of spudcan was penetrated into the footprint soil. Most probably a general shear failure (Terzaghi, 1943) developed in soil under the spudcan. Due to the unbalanced geometry of the footprint surface under the spudcan, the soil was pushed to move toward the footprint crater. The passive soil wedge below the left flange of the spudcan induced a horizontal reaction force which acted toward the x-axis direction. Under the spudcan, the in-filled ground on the left, caused the vertical reaction force V_r to shift to the left of the tip cone. The eccentric V_r generated a clockwise reaction moment M_r about the L.R.P. of the spudcan. The sign convention for V, H, and M in this study was defined at the end of section 2.1. In Fig. 11 and 12, for $\beta = 0.25D$ and $z = 0.2D$, the measured $H_r = +39$ N and $M_r = -43$ N-m.

In Fig. 15(e), for the case $\beta = 0.5D$ and $z = 0$, the lower cone (with a slope angle of 13°) below the right flange of spudcan had been pushed into the rim of the footprint. However, the left flange of the spudcan was hanging over the footprint slope. In this figure, the vertical reaction force V_r was obviously eccentric, and a counter-clockwise reaction moment M_r was induced about the L.R.P. of the spudcan.

The spudcan-footprint interaction illustrated in Fig. 15(e) was similar to the loading of a footing on or near a slope. Coduto (2001) stated, special concerns for such a situation included: (1) the reduction in lateral support makes bearing capacity failure more likely; (2) the foundation might be undermined if a shallow landslide were to occur; (3) the near-surface soils may be slowly creeping downhill, and this creep may cause the footing to move slowly downslope. For more information regarding bearing capacity of footing on slopes, the reader is refer to Shields *et al.* (1990). In Fig. 15(e), with increasing footing loading, the footprint slope could develop a shallow landslide along the assumed failure surface, and a horizontal reaction force H_r could act on the spudcan. However, the lateral movement of the model spudcan in the laboratory was confined by the steel loading frame, and the spudcan of the TIV in the field could be restrained by the stiffness of its hull. In Fig. 11 and 12 for $\beta = 0.5D$, the measured H_r and M_r were represented by the green dashed curves. At the penetration depth $z = 0$, the recorded $H_r = -7.8$ N and $M_r = +13.7$ N-m.

In Fig. 15(f), for the case $\beta = 0.5D$ and $z = 0.2D$, the spudcan was penetrated into the footprint soil. The induced soil behavior was similar to the general shear failure developed below a

shallow foundation, as indicated in Fig. 15(f). The passive soil wedge below the left flange of the spudcan caused a H_r that acted along the *x*-axis direction. The eccentric V_r generated a clockwise reaction moment about the L.R.P.. In Fig. 11 and 12, for β = 0.5*D* and *z* = 0.2*D*, the measured H_r = +25.0 N and M_r = −25.8 N-m. It could be concluded that the unusual reversal of horizontal reaction force and reaction moment in Fig. 11 and 12 was induced by different failure mechanisms in foundation soil at different penetration stages.

In Fig. 15(g) and 15(h), for the case β = 2.0*D*, the location of re-penetration was far from that of the first penetration. The re-penetration of the spudcan should be independent of the existing footprint induced by the first penetration. The reactions V_r, H_r, and M_r induced by the re-penetration should be exactly the same as the reactions induced by the first penetration. In Fig. 11 and 12, for β = 2.0*D*, the measured H_r and M_r were represented by the brown dashed curves. In Fig. 11 and 12, at both *z* = 0 and *z* = 0.2*D*, the measured H_r and M_r for the axisymmetric re-penetration were zero.

5.3 Effects of Offset Distance

Based on their centrifuge test results, Kong *et al.* (2013) reported, for the spudcan penetrating clay with an manually cut footprint, the maximum horizontal force and maximum moment peak at an offset distance β = 1.0*D*. This finding was in good agreement with results published by Stewart and Finnie (2001), Cassidy *et al.* (2009), and Gan (2009), who all reported critical offset distances between 0.5*D* and 1.0*D*.

Figure 16 showed the variation of vertical reaction force V_r measured at different penetration depths (*z*/*D* = 0.1, 0.15, and 0.2) as a function of normalized offset distance (β/*D* = 0, 0.125, 0.25, 0.5, 1.0, 1.5, and 2.0). For the offset distance β = 0, due to "stamp-on-void" situation, no vertical reaction force on the spudcan was measured at the penetration depth of 0.10*D*. However, with increasing offset distance β, the vertical reaction V_r measured at the penetration depth 0.10*D* and 0.15*D* rapidly build up. For an offset distance β equal to or greater than 1.0*D*, the effects of β on the measured vertical reaction became insignificant.
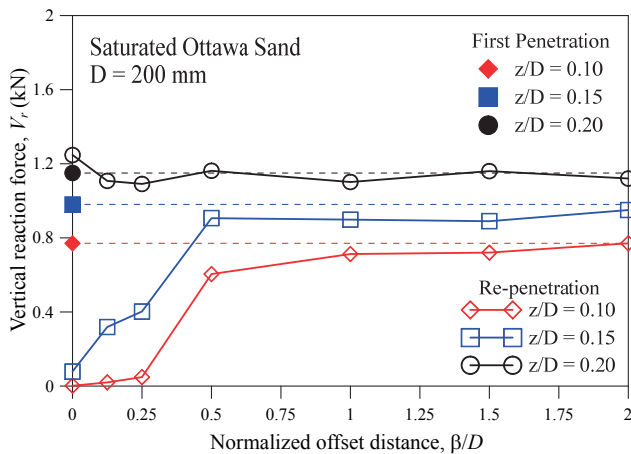
Figure 17 showed the variation of horizontal reaction force H_r as a function of normalized offset distance. At the penetration depth *z* = 0.20*D*, the maximum horizontal reaction appeared at the offset distance β = 0.25*D*. At the penetration depth *z* = 0.15*D*, the maximum horizontal reaction $H_{r,max}$ peaked at an offset distance 0.5*D*. Figure 18 indicated the variation of reaction moment M_r as a function of normalized offset distance. At the penetration depth *z* = 0.20*D*, the absolute maximum reaction moment $M_{r,max}$ peaked at the offset distance β = 0.25*D*. At the penetration depth *z* = 0.15*D*, the absolute $M_{r,max}$ peaked at the offset distance β = 0.50*D*. It could be concluded that, for the re-penetration of a spudcan near an existing footprint on sand, the critical offset distance varied between 0.25*D* and 0.50*D*. The critical offset distance was influenced by both the penetration depth and the type of seabed soil.

It could be concluded from the test data in Fig. 16 to 18 that, when the point of re-penetration was at least 2.0*D* from the first penetration, the effects of the existing footprint disappeared. The re-penetration became independent of the first penetration, as illustrated in Fig. 19(a) and 19(b). This finding was in fairly good agreement with the general guideline C6.4.2 by SNAME (2008): it is usually acceptable for a spudcan to be installed at minimum distance (from the edge of the bearing area to the edge of the footprint) of one diameter (1*D*) measured at the spudcan bearing area.
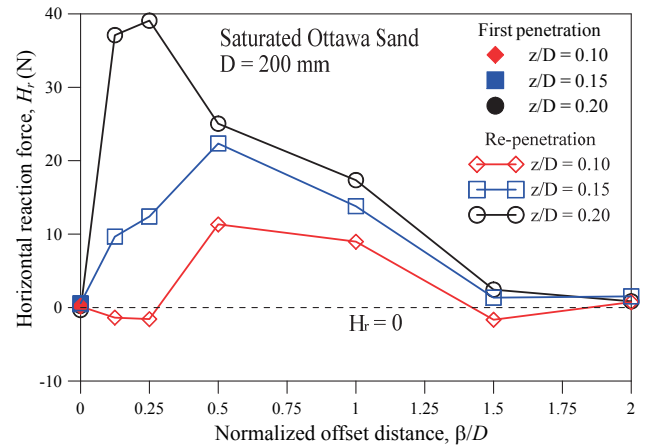

Fig. 17 Variation of horizontal reaction on spudcan due to re-penetration at different offset locations
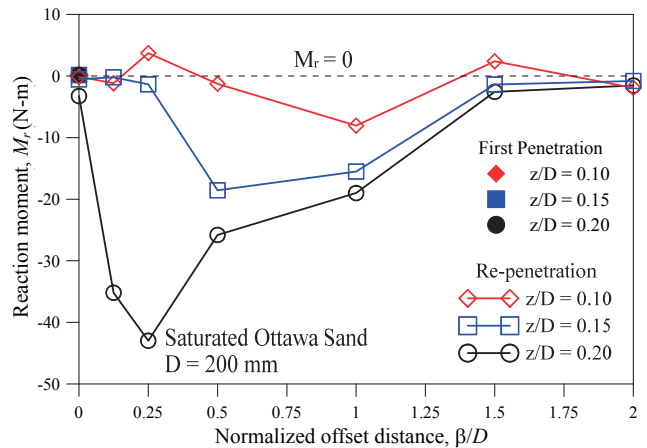

Fig. 16 Variation of vertical reaction on spudcan due to re-penetration at different offset locations

Fig. 18 Variation of reaction moment on spudcan due to re-penetration at different offset locations
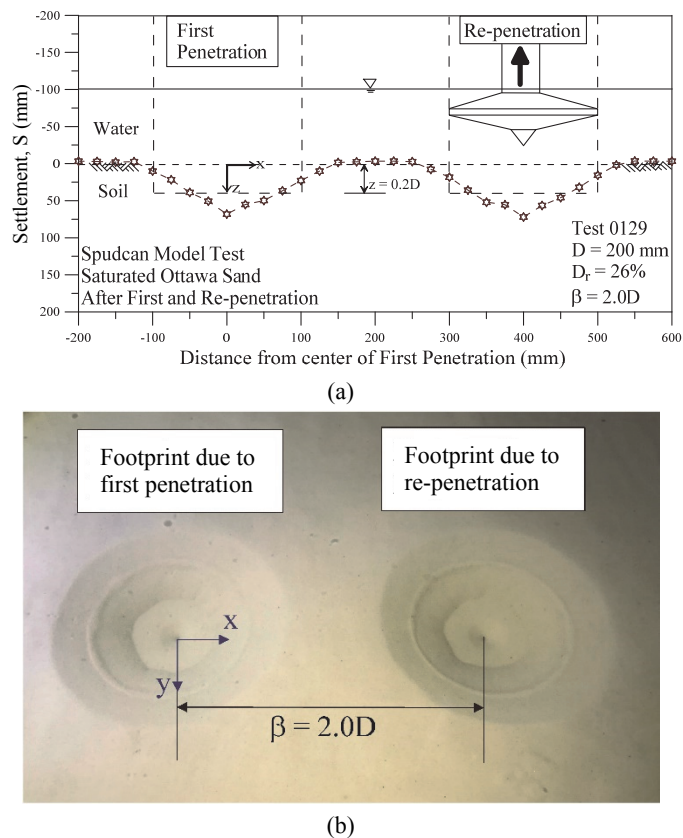
(a)

(b)

Fig. 19   Independent footprints after first and re-penetration of spudcan at offset distance β = 2.0*D*

5.4   Limitations

In this study, the major limitation of the findings obtained from the 1-g physical model tests was the scale effect. For example, the area of the spudcan of the turbine installation vessel named "Torben" shown in Fig. 2 was 90 m². Assuming the spudcan was circular, the corresponding diameter of the spudcan would be 10.7 m. With a prototype condition of a 10.7 m-diameter spudcan, for a model spudcan with the diameter of 0.2 m, the length scaling factor n = 53.5 was adopted for all model tests in this study. Other physical quantities for the model experiments could be computed based on the scaling law shown in Table 1. The minute force and moment on the spudcan during penetration in the 1-g physical model could not fully simulate the force and moment on the spudcan in the field. It should be noted that, in this study only observations regarding the failure mechanism and related soil behavior were emphasized. It is obvious that more investigation based on centrifuge experiments, numerical studies, and full-scale tests associated with this subject are needed.

Table 1   Scaling law (after Wood *et al.* 2002)

Variable	Scaling factor for 1g model
Density	1
Diameter	$1/n$
Displacement	$1/n$
Force	$1/n^2$
Moment	$1/n^3$

Other limitations of this study included that only a horizontal seabed with a single sandy layer was considered. Only the vertical penetration loading was applied on the spudcan, the horizontal force and bending moment due to ocean current, wind load, and earthquake excitation were neglected.

6.   CONCLUSIONS

Based on the analytical and experimental results obtained during this investigation, the following conclusions were drawn regarding the re-penetration of a spudcan on sand near an existing footprint.

Theoretical estimation based on the bearing capacity equation suggested by SNAME (2008) indicated that, the penetration depth of the spudcan was influenced by the vertical load applied, spudcan diameter, shear strength of the soil, and most of all: the type of seabed soil.

For the first penetration of the spudcan, the measured vertical reaction force on the spudcan was in fairly good agreement with the theoretical solution based on SNAME (2008). When the spudcan was extracted from the sandy soil, the vertical reaction force on the spudcan suddenly vanished. The upward-moving spudcan was separated from discrete soil particles below. During the penetration of the axisymmetric spudcan, the measured horizontal reaction and reaction moment on the spudcan were negligible.

For the spudcan re-penetration with an offset distance β = 0 at the penetration depth from 0 to 0.1*D*, due to the existence of the footprint depression, the spudcan was in a "stamp-on-void" condition, all reactions on the spudcan were zero. However, after the spudcan bearing surface was embedded in soil at the penetration depth of 0.15*D*, because the footprint soil had been heavily compressed and sheared during the first penetration, the measured vertical reaction increased rapidly with increasing depth of penetration. At the penetration depth of 0.2*D*, the measured vertical reaction force was nearly the same as that due to the first penetration. Since both penetration were axisymmetric, the measured horizontal reaction force and moment reaction on the spudcan were negligible.

For the re-penetration with offset distance β = 0.5*D* at the penetration depth z = 0, the spudcan-footprint interaction was similar to the loading of a footing on or near a slope. The induced vertical reaction force was eccentric, and a reaction moment about the L.R.P. was induced. A negative horizontal reaction force and a positive reaction moment on the spudcan were measured.

For the case with an offset distance β = 0.5*D* at the penetration depth z = 0.2*D*, the induced soil behavior was similar to the general shear failure below a shallow foundation. When the spudcan was pushed down, soil below moved along the rupture surface. The passive Rankine wedge pushed the soil to fill the existing footprint. A positive horizontal reaction force and a negative reaction moment on the spudcan were measured. The unusual reversal of horizontal reaction and reaction moment with increasing depth of penetration was induced by different failure mechanisms in foundation soil at different penetration stages.

When the offset distance was greater than twice the spudcan diameter, the effects of the existing footprint disappeared. The re-penetration became independent of the first penetration. This finding was in good agreement with the general guideline C6.4.2 by SNAME (2008).

For the re-penetration of spudcan in a sandy seabed, the critical offset distances varied between 0.25*D* and 0.50*D*. The critical offset distance was influenced by both the penetration depth and the type of seabed soil.

ACKNOWLEDGMENTS

REFERENCES

ASTM International (2014). *ASTM D4254-91, Standard Test Method for Minimum Index Density and Unit Weight of Soils and Calculation of Relative Density.* West Conshohocken, PA, U.S.A. https://standards.globalspec.com/std/9996935/ASTM%20D4254

Bureau of Energy (2016). *2016 Annual Report of the Bureau of Energy*, Ministry of Economic Affairs, Taipei, Taiwan (in Chinese). https://www.moeaboe.gov.tw/ECW/populace/content/ContentLink.aspx?menu_id=137&sub_menu_id=358

Cassidy, M.J. and Bienen, B. (2002). "Three-dimensional numerical analysis of jack-up structures on sand." *Proceedings of the 12th International Offshore and Polar Engineering Conference*, 26-31 May, Kitakyushu, Japan, Paper No. 2002-JSC-355, 1-8.

Cassidy, M.J., Quah, C.K., and Foo, K.S. (2009). "Experimental investigation of the reinstallation of spudcan footings close to existing footprints." *Journal of Geotechnical and Geoenvironmental Engineering*, ASCE, **135**(4), 474-486. https://doi.org/10.1061/(ASCE)1090-0241(2009)135:4(474)

Coduto, D.P. (2001). *Foundation Design: Principles and Practice,* 2nd Ed., Prentice Hall, Englewood Cliffs, NJ, U.S.A.

Das, B.M. and Sobhan, K. (2018). *Principle of Foundation Engineering,* 9th Ed., Cengage Learning, Boston, U.S.A. https://www.cengage.com/c/principles-of-geotechnical-engineering-9e-das

Dier, A., Carrol, B., and Abolfathi, S. (2004). *Guidelines for Jack-Up Rigs with Particular Reference to Foundation Integrity*. Research Report 289, Health and Safety Executive, U.K. http://www.hse.gov.uk/research/rrpdf/rr289.pdf

Fang, Y.S., Cheng, L., Chen, S.L., and Shih, Y.C. (2019). "Penetration resistance of jack-up spudcan on dense sand overlying loose sand." *Journal of GeoEngineering,* **14**(3), 129-139.

Gan, C.T. (2009). *Centrifuge Model Study on Spudcan-Footprint Interaction*. Ph.D. Dissertation, National University of Singapore, Singapore. http://scholarbank.nus.edu.sg/handle/10635/17338

Gan, C.T., Leung, C.F., Cassidy, M.J., Gaudin, C., and Chow, Y.K. (2012). "Effect of time on spudcan-footprint interaction in clay." *Géotechnique*, **62**(5), 401-413. https://doi.org/10.1680/geot.10.P.063

Hartono (2014), *Centrifuge Model Study on Spudcan-Footprint Remediation Techniques*. Ph.D. Dissertation, National University of Singapore, Singapore. http://scholarbank.nus.edu.sg/handle/10635/118293

Hartono, Tho, K.K., Leung, C.F., and Chow, Y.K. (2014). "Centrifuge and numerical modelling of reaming as mitigation measure for spudcan-footprint interaction." *Proceedings of the Offshore Technology Conference Asia*, 25-28 March, Kuala Lumpur, Malaysia. https://doi.org/10.4043/24835-MS

Hossain, M.S., Randolph, M.F., Hu, Y., and White, D.J. (2006). "Cavity stability and bearing capacity of spudcan foundations on clay." *Proceedings of the Offshore Technology Conference,* OTC 17770, Houston, Texas, U.S.A., 1-18. https://doi.org/10.4043/17770-MS

Kong, V.W. (2011), *Jack-up Reinstallation near Existing Footprints*. Ph.D. Dissertation, University of Western Australia, Perth, Australia. https://api.research-repository.uwa.edu.au/portalfiles/portal/3380341/Kong_Vickie_Waiwah_2011.pdf

Kong, V., Cassidy, M.J., and Gaudin, C. (2013). "Experimental study of effect of geometry on reinstallation of jack-up next to footprint." *Canadian Geotechnical Journal*, **50**, 557-573. https://doi.org/10.1139/cgj-2012-0381

Lo Presti, D.C.F., Pedroni, S., and Crippa, V. (1992). "Maximum dry density of cohesionless soils by pluviation and by ASTM D4253-83: A comparative study." *Geotechnical Testing Journal,* **15**(2), 180-189. https://doi.org/10.1520/GTJ10239J

Marine Traffic (2017). *Global Ship Tracking Intelligence*. https://www.marinetraffic.com/zh/ais/details/ships/shipid:153094/mmsi:9578256/vessel:TORBEN

Martine, C.M. and Houlsby, G.T. (2000). "Combined loading of spudcan foundations on clay: laboratory tests." *Geotechnique*, **50**(4), 325-338. https://doi.org/10.1680/geot.2000.50.4.325

Meyerhof, G.G. (1963). "Some recent research on the bearing capacity of foundations." *Canadian Geotechnical Journal*, **1**, 16-26. https://doi.org/10.1139/t63-003

Osborne, J.J. (2005). "Are we good or are we lucky?" Presentation Slides for *OGP/CORE Workshop: The Jackup Drilling Option – Ingredients for Success*, National University of Singapore, 26-28 October 2005, Singapore.

Osborne, J.J., Teh, K.L., Houlsby, G.T., Cassidy, M.J., Bienen, B., and Leung, C.F. (2011). *Improved Guidelines for the Prediction of Geotechnical Performance of Spudcan Foundations during Installation and Removal of Jack-up Units.* Joint Industry-funded Project, RPS Energy, U.K. http://www.cofs.uwa.edu.au/__data/assets/pdf_file/0009/2466495/InSafeJIP_Guideline_Rev_1c_28Mar11.pdf

Perloff, W.H. (1975). *Pressure Distribution and Settlement. Foundation Engineering Handbook*, Winterkorn, H.F. and Fang, H.Y., Eds., Van Nostrand Reinhold, New York, U.S.A.

Rad, N.S. and Tumay, M.T. (1987). "Factors affecting sand specimen preparation by raining." G*eotechnical Testing Journal,* **10**(1), 31-37. https://doi.org/10.1520/GTJ10136J

Shields, D., Chandler, N., and Garnier, J. (1990). "Bearing capacity of foundations in slopes." *Journal of Geotechnical Engineering*, ASCE, **116**(3), 528-537. https://doi.org/10.1061/(ASCE)0733-9410(1990)116:3(528)

Society of Naval Architects and Marine Engineers (SNAME) (2008). *Guideline for Site Specific Assessment of Mobile Jack-Up Units*. Technical and Research Bulletin 5-5A, Jersey City, NJ, U.S.A. https://www.proceedings.com/0131.html

Stewart, D.P. and Finnie, I.M.S. (2001). "Spudcan-footprint interaction during jack-up workovers." *Proceedings of the 11th International Offshore and Polar Engineering Conference*, Stavanger, Norway, 61-65.

https://www.onepetro.org/conference-paper/ISOPE-I-01-011

Swancor (2017). "Green energy and environmental protection and safety." Nantou, Taiwan.
http://www.swancor.com/tw/project.php?act=prolist_view&no=94

Taiwan Power Company (2009). *Geological and Bathymetric Investigation Report. Feasibility Study Changhua Offshore Wind Energy, Appendix II* (in Chinese).

Terzaghi, K. (1943). *Theoretical Soil Mechanics.* John Wiley and Sons, Hoboken, NJ, USA.
https://onlinelibrary.wiley.com/doi/book/10.1002/97804701

72766

Wood, D. M., Crewe, A., and Taylor, C. (2002). "Shaking table testing of geotechnical models." *International Journal of Physical Modeling in Geotechnics*, **2**(1), 1-13.
https://doi.org/10.1680/ijpmg.2002.020101

Yi, J.T., Lee, F.H., Goh, S.H., Li, P.Y., and Zhang, X.Y. (2012). "Effective-stress finite element analysis of spudcan penetration." *Proceedings of the ASME2012 31st International Conference on Ocean, Offshore & Arctic Engineering*, OMAE2012, Rio de Janerio, Brazil.
http://doi:10.1115/OMAE2012-83138